

Effect of doping on SGS and weak half-metallic properties of inverse Heusler Alloys

R. Dhakal^a, S. Nepal^a, R. B. Ray^{a,b}, R. Paudel^c, G. C. Kaphle^{a,*}

^aCentral Department of Physics, Tribhuvan University, Kathmandu, Nepal

^bDepartment of Physics, Amrit Campus, T. U., Kathmandu, Nepal

^cSchool of Materials Science and Engineering, Harbin Institute Of Technology, Harbin, 150001, China

Abstract

Heusler alloys with Mn and Co have been found to exhibit interesting electronic and magnetic properties. Mn_2CoAl is well known SGS compound while Mn_2CoGa has weak half metallic character. By using plane wave pseudo-potential method, we studied the effect of Fe and Cr doping on half-metallicity and magnetism of these compounds. The doping destroys the SGS nature of Mn_2CoAl while the small-scale doping enhance the half-metallicity of Mn_2CoGa making it perfect half-metal. In case of Mn_2CoAl , the doping decrease the band gap while increase in band width is noticed for Mn_2CoGa . The half-metallicity is destroyed in both cases when the doping level is beyond certain degree. Moreover, we have also computed magnetic behavior of Mn_2CoZ alloys and we found that total magnetic moments of doped samples have higher values than that of pristine compounds.

Keywords: Inverse Heusler alloys, SGS, Half-Metallicity, Electronic structure, spintronics

1. Introduction

In last two decades, Heusler alloys have been studied extensively because of its diverse magnetic phenomena. Spin gapless [1] and half metallic properties[2] have been reported and SGS is verified experimentally[3] in Heusler family, the importance of which lies in its potential application in the realm of spintronics. The two spin channels show entirely contrasting behavior in half metallic and spin gapless materials which helps to manipulate the charge carriers and should enhance the performance of magnetoelectronic devices such as giant magnetoresistance spin-valves[4], magnetic tunneling junctions[5], spin-injecting[6] and spin transfer torque devices[7]. Moreover, the research on Heusler alloys optical properties have also drawn significant attention though optoelectronic properties is widely studied in perovskite[8–10].

Various theoretical approach to study the phase stability[11], thermal, mechanical and structural properties[12][13] of Heusler alloys has appeared in literature but Heusler alloys containing Mn and Co have attracted particular attention because of the high Curie temperature and peculiar

behavior of magnetic moment of Manganese atom. The neighboring atoms dictate the magnetic moment alignment of Manganese atom[2][14] and the exchange interaction between Mn and Co is found to be short-range effect[15]. The first experimental study of Mn_2CoZ compound was made by Liu *et al.*[2], where they predicted Mn_2CoAl as half metallic and Mn_2CoGa as weakly half-metallic. Later it was revealed that Mn_2CoAl possesses spin gapless property[3] whereas weak half-metallic behavior of Mn_2CoGa was corroborated by further investigation[16]. Mn_2CoZ compounds crystallize in inverse Heusler structure with space group $\bar{F}43m(216)$ [17, 18], where the sequence of atom is Mn-Mn-Co-Z on the diagonal basis, the structure prototype of Hg_2CuTi alloy. In this symmetry, the Mn atoms occupy $A(0,0,0)$ and $B(\frac{1}{4}, \frac{1}{4}, \frac{1}{4})$ sites, whereas Co and Z atoms take $C(\frac{1}{2}, \frac{1}{2}, \frac{1}{2})$ and $D(\frac{3}{4}, \frac{3}{4}, \frac{3}{4})$ sites respectively in Wyckoff positions[19].

The theoretical explanation of the effect of doping and disorder on the properties like SGS and half-metallicity of Heusler alloys has appeared in literature [20][21] but little attention has been given to the weak-half metallic character and the effect of doping on this particular property. In our work, we report the effect of doping on SGS and weak half metallicity of inverse Heusler alloy. For this purpose we chose the conventional cell of Mn_2CoZ ($Z=\text{Al, Ga}$) compounds, where the partial doping is done by Fe and Cr at two different levels. The site occupation of the dopant

*Corresponding author

Email addresses: ramesh.dhakal91@gmail.com (R. Dhakal), sashinepal@gmail.com (S. Nepal), ray_rb@ymail.com (R. B. Ray), gck223@gmail.com (R. Paudel), ramesh.dhakal91@gmail.com (G. C. Kaphle)

atoms is determined by the general empirical rule as described in literature[14] and the unusual site occupation of chromium has also been considered[22].

The general rule is if the dopant atoms have more valance electrons than that of Manganese atoms, then it will occupy A and C sites whereas if the valance electrons of dopant is less than that of Mn atoms, B and D sites will be preferred. But the Cr atoms as a dopant do not obey this rule and prefer to occupy A and C sites. So in our case, both Fe and Cr atoms will occupy the A sites whereas the displaced Mn(A) atoms at A sites will replace the Al(D) or Ga(D) atoms at D sites. During this modeling, it is assumed that the lattice constant of a crystal has not changed due to doping. Also, it is assumed that structural phase transition has not taken place so that the crystal remains in a cubic structure.

2. Computational Details

The electronic and magnetic properties were calculated using plane-wave pseudopotential method within DFT framework implemented using Quantum ESPRESSO package[23, 24]. In our work, for Manganese, Aluminium and Iron atoms Projector-Augmented Wave(PAW) set was used and for Cobalt and Chromium atoms ultra-soft pseudopotential was exploited. Exchange-correlation functional was approximated using Ernzerhof generalized gradient approximation (PBEsol GGA)[25][26, 27]. Cutoff energy for plane-wave was set to 160 Ry for Mn_2CoGa and 175 Ry for Mn_2CoAl . For k-point sampling in electronic structure calculation, we used Monkhorst-pack grid of size $8 \times 8 \times 8$ for primitive cell and $6 \times 6 \times 6$ for conventional cell. Linear tetrahedral integration method is used to calculate density of states[28]. Lattice parameter was optimized using total energy minimization method. For doping, we used conventional structure with 16 atoms/cell. Coordinate relaxation was performed until total energy change between two consecutive scf step is less than 1×10^{-5} Ry. Force convergence threshold was set to 1×10^{-3} Ry/a.u.

3. Results and Discussion

The structural stability of compounds under study is confirmed by the calculation of formation and cohesive energy. The formation and cohesive energy for $Mn_2CoM_xZ_{1-x}$ [M=Cr,Fe & Z=Al,Ga & x=0,0.25,0.5] can be written as

$$E_{Form}^{Mn_2CoM_xZ_{1-x}} = E_{tot} - (2E_{Mn}^B + E_{Co}^B + E_M^B + E_Z^B) \quad (1)$$

$$E_{Coh}^{Mn_2CoM_xZ_{1-x}} = E_{tot} - (2E_{Mn} + E_{Co} + E_M + E_Z) \quad (2)$$

Here, $E_{Form}^{Mn_2CoM_xZ_{1-x}}$ and $E_{Coh}^{Mn_2CoM_xZ_{1-x}}$ represent the formation and cohesive energy of the compounds respectively whereas E_{tot} is the total energy per formula unit. In equation 1, E_{Mn}^B , E_{Co}^B , E_M^B and E_Z^B indicate total energy per atom for bulk whereas in equation 2 E_{Mn} , E_{Co} , E_M and E_Z represents the total energy of corresponding isolated atom. From table 1, we can see that cohesive energy of all the compounds, pristine as well as doped sample, are negative which confirms the structural stability of our compounds.

Fig. ?? represents the spin resolved band structure of Mn_2CoZ compounds near the Fermi level. The meticulous explanation of band structure can be done by invoking the hybridization scheme [29] suggested by Galanakis *et al.* for inverse Heusler alloys. The knowledge of Slater Pauling rule of full Heusler structure [30] would be of great assistance while we are dealing with the hybridization scheme of inverse structure.

The close look of spin up channel of Mn_2CoAl around the fermi level shows that t_{1u} and e_g bands just touch the fermi level at point Γ and X respectively making it a strong candidate for Spin Gapless material. The spin down channel shows usual indirect band gap around the Fermi level. The gap of 0.358 eV is measured between the upper valence band at Γ and lower conduction band at X.

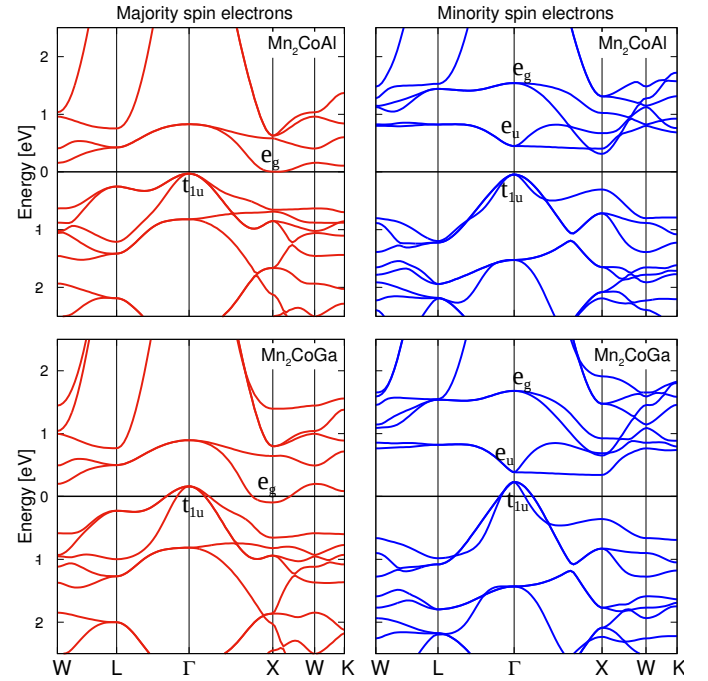


Figure 1: Calculated band structure of Mn_2CoAl and Mn_2CoGa for Majority (red) and Minority (blue) channel at lattice constant of 5.6506Å and 5.6695Å respectively.

In case of Mn_2CoGa , the metallic nature is dominant for majority spin electrons (see Fig. ??) due to the inter-

Table 1: Formation energy and cohesive energy of compounds under study.

Alloy	$E_{form}(\text{eV/atom})$	$E_{coh}(\text{eV/atom})$
Mn_2CoAl	-0.286	-5.000
$\text{Mn}_2\text{CoCr}_{0.25}\text{Al}_{0.5}$	-0.190	-4.956
$\text{Mn}_2\text{CoCr}_{0.5}\text{Al}_{0.5}$	-0.123	-4.941
$\text{Mn}_2\text{CoFe}_{0.25}\text{Al}_{0.5}$	-0.206	-5.038
$\text{Mn}_2\text{CoFe}_{0.5}\text{Al}_{0.5}$	-0.132	-5.082
Mn_2CoGa	-0.192	-4.725
$\text{Mn}_2\text{CoCr}_{0.25}\text{Ga}_{0.5}$	-0.123	-4.754
$\text{Mn}_2\text{CoCr}_{0.5}\text{Ga}_{0.5}$	-0.078	-4.806
$\text{Mn}_2\text{CoFe}_{0.25}\text{Ga}_{0.5}$	-0.133	-4.829
$\text{Mn}_2\text{CoFe}_{0.5}\text{Ga}_{0.5}$	-0.079	-4.938

section of t_{1u} and e_g bands around the Fermi level while the band gap of 0.113 eV is measured for spin down channel. The valence band maximum i.e. t_{1u} lies slightly above the Fermi level indicating weak half metallic character of Mn_2CoGa . In both cases, the band structure in the energy range of -2.5eV to 0eV are mainly due to the d -electrons of the Manganese and Cobalt atoms. The scattered nature of bands in this region is predominantly due to the the strong hybridization between Manganese-Cobalt and Manganese-Manganese d -electrons but there is also the contribution of p -electrons from Al and Ga atoms. The low-lying s bands are not shown in the figure.

Since, by the transformation rule [29][30], t_{1u} and e_u states do not contain any d -orbitals of Mn(B) atoms, the d hybrids of these states are localized on Mn(A) and Co atoms. This is the reason why the states around the Fermi level are localized on Mn(A) and Co atoms. The gap between Mn(A) and Co is d - d band gap due to e_u - t_{1u} splitting.

From Fig. ??, in case of pristine Mn_2CoAl , we can see that the dos around the Fermi level shows valley approaching zero peak indicating zero width energy gap supporting the SGS nature of band structure. For minority charge carriers, there are no states around the fermi level, suggesting its semi conducting behavior. The dos of Mn_2CoGa shows the metallic nature of majority electrons whereas very small amount of density of states appeared around the Fermi level for the minority states. This indicates that the pristine Mn_2CoGa may not have 100% spin polarization at Fermi level, as in the case of half-metal. Now, let us focus on the band gap of Mn_2CoZ ($Z=\text{Al, Ga}$) compounds. We can see clearly that the band gap of pristine Mn_2CoAl is larger than the gap width of Mn_2CoGa . Liu *et al.*[2] have shown that smaller the value of lattice con-

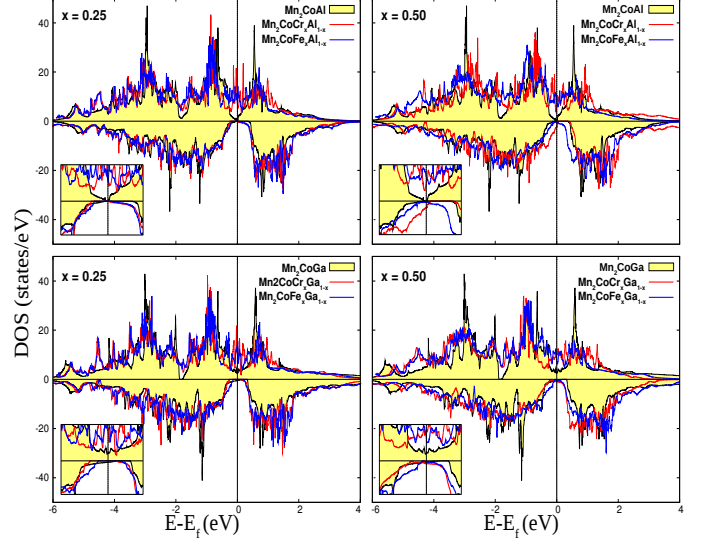


Figure 2: Spin resolved total density of states(DOS) of Mn_2CoAl and Mn_2CoGa for conventional cell at 5.6506Å and 5.6695Å respectively. Blue line represents Fe doping while red line denotes Cr doping on Mn_2CoZ ($Z=\text{Al, Ga}$) compounds.

stant larger will be the band gap and vice versa, which is in good agreement with our case. The gap width largely depends upon the hybridization of delocalized p -electrons from the Z atoms and localized d -electrons of Manganese and Cobalt atoms. Since, the binding energy of p electrons of Al is more than that of Ga atoms, the gap width of Mn_2CoAl is larger than that of Mn_2CoGa .

The blue line indicates Fe doping while the red line represents Cr doping in Fig. ???. The changes around the Fermi level is interesting and the modification in band gap is important for the study of different phenomena. For 25% doping, the careful inspection around the Fermi level clearly shows that the SGS property of Mn_2CoAl has been destroyed and weak-half metallic nature of Mn_2CoGa has disappeared introducing half-metallic nature in both cases making doped Mn_2CoZ compound a strong candidate of half-metal.

For Mn_2CoAl , 25% doping of Fe or Cr decrease the band gap in comparison to its pristine form shifting the band gap on the left side but somehow half-metallicity is preserved. The band gap is measured to be 0.243 eV and 0.254eV for Fe and Cr doping respectively which is smaller than the minority band gap in pure Mn_2CoAl . The narrowing of band gap is more in case of Fe doping than Cr doping. This can be explained by invoking the exchange splitting and coulomb repulsion competition, as we go on adding the electrons in the system through Fe doping. In case of Fe doping, in order to preserve half metallicity, the extra electron from Fe must occupy anti-

Table 2: Individual and total spin magnetic moments of Mn_2CoAl compound in case of Fe and Cr doping in μ_B . * represents the changed value of spin magnetic moments of individual atoms after doping.

Compounds	Mn(A)	Mn(B)	Mn*(B)	Co(C)	Co*(C)	Cr(A)	Fe(A)	Mn(D)	Al(D)	Total
Mn_2CoAl	-1.1996	2.3152	-	0.9379	-	-	-	-	-0.03109	8.00
$\text{Mn}_2\text{CoCr}_{0.25}\text{Al}_{0.75}$	-0.9640	2.6897	2.1677	1.1214	1.0975	-1.3381	-	1.8923	-0.0356	11.00
$\text{Mn}_2\text{CoCr}_{0.5}\text{Al}_{0.5}$	-0.8526	2.5303	1.9578	1.2969	1.2810	-1.2959	-	1.9786	-0.0417	13.56
$\text{Mn}_2\text{CoFe}_{0.25}\text{Al}_{0.75}$	-1.1586	2.7074	2.1376	1.1532	0.9793	-	1.0844	2.0216	-0.0388	13.00
$\text{Mn}_2\text{CoFe}_{0.5}\text{Al}_{0.5}$	-1.4142	2.4943	2.0041	1.3679	1.1740	-	1.2164	2.1179	-0.0513	17.82

Table 3: Individual and total spin magnetic moments of Mn_2CoGa compound in case of Fe and Cr doping in μ_B . * represents the changed value of spin magnetic moments of individual atoms after doping.

Compounds	Mn(A)	Mn(B)	Mn*(B)	Co(C)	Co*(C)	Cr(A)	Fe(A)	Mn(D)	Ga(D)	Total
Mn_2CoGa	-1.3611	2.4897	-	0.9131	-	-	-	-	-0.0152	8.14
$\text{Mn}_2\text{CoCr}_{0.25}\text{Ga}_{0.75}$	-1.2148	2.8293	2.3434	1.1164	1.0592	-1.4877	-	2.1053	-0.0204	11.00
$\text{Mn}_2\text{CoCr}_{0.5}\text{Ga}_{0.5}$	-1.0929	2.6714	2.1038	1.3117	1.2535	-1.4223	-	2.1292	-0.0257	13.79
$\text{Mn}_2\text{CoFe}_{0.25}\text{Ga}_{0.75}$	-1.4142	2.8055	2.2731	1.1515	0.8991	-	1.1740	2.1408	-0.0254	13.00
$\text{Mn}_2\text{CoFe}_{0.5}\text{Ga}_{0.5}$	-1.5800	2.6573	2.0072	1.3700	1.1351	-	1.1975	2.1959	-0.0404	17.95

bonding majority states. Since these states have relatively higher energy than minority states, energetically it is not very approbative. Thus, the new states appears on the unoccupied minority states, the state which we can see in Fig. ?? near the edges of the gap, reducing the gap width of doped Mn_2CoAl .

In case of Mn_2CoGa , the doping gives different result. For 25% doping of Fe or Cr, increase in the gap width is noticed unlike Mn_2CoAl . The gap width is 0.307eV for Fe doping while the value increased to 0.352eV for Cr doping. This peculiar behavior of Mn_2CoGa is beyond the scope of this paper and is the matter of further investigation. We hope this anomalous behavior will attract the attention of other researcher in this field.

In table 2 and 3 we have presented the total and individual spin magnetic moments of the Mn_2CoZ compounds. From table, it is clear that the ground state magnetic structure of Mn_2CoZ compounds is ferri-magnetic. Magnetic moment of Mn and Co at B and C sites are anti-ferromagnetically aligned with that of Mn and Z at A and D sites. It is important to note that the Manganese atom at B site has highest value of spin magnetic moment which ferromagnetically couples with Cobalt atoms whose spin moment is near to unity. The reason for the ferromagnetic and antiferromagnetic alignment of different atoms in inverse Heusler alloy is described in reference [2].

In case of Mn_2CoAl , the total magnetic moment follows the Slater-Pauling rule, the rule which is important to analyze the electronic properties by studying the magnetic properties. The total number of valence electrons in

Mn_2CoAl is 26, which is the sum of spin up and spin down electrons. Among 26 electrons, the 12 are in spin down states whereas 14 are in spin up states. These two extra electrons in spin up states are responsible for the magnetic moment of Mn_2CoAl . The conventional cell in this case is four times the primitive cell, so there would be total 8 extra electrons in spin up states giving total spin magnetic moment of $8\mu_B$. But for Mn_2CoGa , as the upper valence state of minority electrons just cross the Fermi level (see Fig. ??), we do not get the exact integer value for total spin magnetic moment, which can be verified from the table.

It is interesting to note that for 25% doping, in all cases, there is an integer value of total spin magnetic moment, the strong evidence of the inducement of half-metallic properties in the doped samples. The non-integer value of total spin magnetic moment of 50% doped samples support the fact that half-metallic properties is destroyed for large degree of doping.

From table 2 and 3, we can see that the spin magnetic moment alignment of Cr(A) and Mn(A) is in same direction whereas in case of Fe doping unlike Cr(A), Fe(A) and Mn(A) are anti-ferromagnetically aligned. This is the reason why the total spin magnetic moment value in Fe doped samples is more than for the Cr doped samples. Here, it has to be noted that in every doped sample the value of total spin magnetic moments is more than that of pristine compound. The observed increase in magnetic moment value in doped sample could be explained by taking into account the change in local environment of certain individual atoms by the disorder produced from dopant atoms.

The change in the magnetic moment of particular individual atoms sum up ultimately giving the increased value of magnetic moment of doped sample. Particularly, when we dope Fe or Cr, it occupies A site in accordance with general occupation rule and displace the Mn(A) atoms. These displaced Mn(A) atoms occupy the D sites and while doing so the anti-ferromagnetic alignment of Mn(A) atoms change to ferromagnetic alignment which largely increase the total spin magnetic moment value. Thus, the lion's share of credit for the increase in total magnetic moment goes to the Manganese atom.

4. Conclusion

In our work, we have carried out the first principle study to investigate the effect of doping on SGS and weak half metallic properties of inverse Heusler alloys. For this, we have taken Mn_2CoZ (Al, Ga) compounds where Fe and Cr atoms were doped at two different concentration. We have found that the low degree doping enhance the half metallic properties in inverse Heusler alloys where as doping beyond certain degree destroys half-metallicity. It has been found that the Fe doping decreases the gap width where as Cr doping increase the band gap. The Magnetic moments are found to be drastically increases on doping concentrations accordingly.

References

- [1] S. Skaftouros, K. Özdoğan, E. Şaşıoğlu, I. Galanakis, Search for spin gapless semiconductors: The case of inverse heusler compounds, *Applied Physics Letters* 102 (2013) 022402.
- [2] G. D. Liu, X. F. Dai, H. Y. Liu, J. L. Chen, Y. X. Li, G. Xiao, G. H. Wu, mn_2Coz ($z = \text{Al, Ga, In, Si, Ge, Sn, Sb}$) compounds: Structural, electronic, and magnetic properties, *Phys. Rev. B* 77 (2008) 014424.
- [3] S. Ouadi, G. H. Fecher, C. Felser, J. Kübler, Realization of spin gapless semiconductors: The heusler compound mn_2CoAl , *Phys. Rev. Lett.* 110 (2013) 100401.
- [4] Z. H. Xiong, D. Wu, Z. Valy Vardeny, J. Shi, Giant magnetoresistance in organic spin-valves, *Nature* 427 (2004) 821–824.
- [5] J. Han, G. Gao, Large tunnel magnetoresistance and temperature-driven spin filtering effect based on the compensated ferrimagnetic spin gapless semiconductor Ti_2MnAl , *Applied Physics Letters* 113 (2018) 102402.
- [6] M. E. Jamer, Y. J. Wang, G. M. Stephen, I. J. McDonald, A. J. Grutter, G. E. Sterbinsky, D. A. Arena, J. A. Borchers, B. J. Kirby, L. H. Lewis, B. Barbiellini, A. Bansil, D. Heiman, Compensated ferrimagnetism in the zero-moment heusler alloy mn_3Al , *Phys. Rev. Applied* 7 (2017) 064036.
- [7] D. Kurebayashi, K. Nomura, Theory for spin torque in weyl semimetal with magnetic texture, *Scientific Reports* 9 (2019) 5365.
- [8] Z.-L. Yu, Y.-Q. Zhao, P.-B. He, B. Liu, J.-L. Yang, M.-Q. Cai, The influence of electrode for electroluminescence devices based on all-inorganic halide perovskite CsPbBr_3 , *Journal of Physics: Condensed Matter* 32 (2019) 065002.
- [9] Z.-L. Yu, Q.-R. Ma, B. Liu, Y.-Q. Zhao, L.-Z. Wang, H. Zhou, M.-Q. Cai, Oriented tuning the photovoltaic properties of y-RbGeX_3 by strain-induced electron effective mass mutation, *Journal of Physics D: Applied Physics* 50 (2017) 465101.
- [10] Y.-Q. Zhao, Q.-R. Ma, B. Liu, Z.-L. Yu, J. Yang, M.-Q. Cai, Layer-dependent transport and optoelectronic property in two-dimensional perovskite: $(\text{pea})_2\text{pbI}_4$, *Nanoscale* 10 (2018) 8677–8688.
- [11] H. Rached, D. Rached, R. Khenata, B. Abidri, M. Rabah, N. Benkhetou, S. B. Omran, A first principle study of phase stability, electronic structure and magnetic properties for $\text{Co}_{2-x}\text{Cr}_x\text{MnAl}$ heusler alloys, *Journal of Magnetism and Magnetic Materials* 379 (2015) 84 – 89.
- [12] I. Asfour, H. Rached, S. Benalia, D. Rached, Investigation of electronic structure, magnetic properties and thermal properties of the new half-metallic ferromagnetic full-heusler alloys $\text{Cr}_2\text{GdSi}_{1-x}\text{Ge}_x$: An ab-initio study, *Journal of Alloys and Compounds* 676 (2016) 440 – 451.
- [13] I. Asfour, H. Rached, D. Rached, M. Caid, M. Labair, Magneto-electronic, mechanical and thermodynamic properties of full-heusler alloys $\text{Cr}_2\text{GdGe}_{1-x}\text{Sn}_x$, *Journal of Alloys and Compounds* 742 (2018) 736 – 750.
- [14] Y. J. Zhang, E. K. Li, G. J. (and Liu, J. L. Chen, W. H. Wang, G. H. Wu, Ferromagnetic structures in Mn_2CoGa and Mn_2CoAl doped by Co, Cu, V, and Ti, *Journal of Applied Physics* 113 (2013) 123901.
- [15] L. Feng, L. Ma, Z. Y. Zhu, W. Zhu, E. K. Liu, J. L. Chen, G. H. Wu, F. B. Meng, H. Y. Liu, H. Z. Luo, Y. X. Li, Ferromagnetic exchange interaction between Co and Mn in the heusler alloy CuCoMnAl , *Journal of Applied Physics* 107 (2010) 013913.
- [16] L. Wollmann, S. Chadov, J. Kübler, C. Felser, Magnetism in cubic manganese-rich heusler compounds, *Phys. Rev. B* 90 (2014) 214420.
- [17] J. Ma, J. He, D. Mazumdar, K. Munira, S. Keshavarz, T. Lovorn, C. Wolverton, A. W. Ghosh, W. H. Butler, Computational investigation of inverse heusler compounds for spintronics applications, *Phys. Rev. B* 98 (2018) 094410.
- [18] W. H. Butler, A. W. Ghosh et. al., Heuslers home url: <http://heusleralloys.mint.ua.edu>,
- [19] T. J. Burch, T. Litrenta, J. I. Budnick, Hyperfine studies of site occupation in ternary systems, *Phys. Rev. Lett.* 33 (1974) 421–424.
- [20] I. Galanakis, K. Özdoğan, E. Şaşıoğlu, S. Blügel, Conditions for spin-gapless semiconducting behavior in Mn_2CoAl inverse heusler compound, *Journal of Applied Physics* 115 (2014) 093908.
- [21] I. Galanakis, K. Özdoğan, B. Aktaş, E. Şaşıoğlu, Effect of doping and disorder on the half metallicity of full heusler alloys, *Applied Physics Letters* 89 (2006) 042502.
- [22] Y. Zhang, G. Li, E. Liu, J. Chen, W. Wang, F. Meng, G. Wu, Atomic site occupation determined by magnetism in the heusler alloy Mn_2CoGa doped with Cr, *Physica B: Condensed Matter* 454 (2014) 1 – 7.
- [23] P. Giannozzi, S. Baroni, N. Bonini, M. Calandra, R. Car, C. Cavazzoni, D. Ceresoli, G. L. Chiarotti, M. Cococcioni, I. Dabo, A. D. Corso, S. de Gironcoli, S. Fabris, G. Fratesi, R. Gebauer, U. Gerstmann, C. Gougousis, A. Kokalj, M. Lazzeri, L. Martin-Samos, N. Marzari, F. Mauri, R. Mazzeo, S. Paolini, A. Pasquarello, L. Paulatto, C. Sbraccia, S. Scandolo, G. Sclauzero, A. P. Seitsonen, A. Smogunov,

- P. Umari, R. M. Wentzcovitch, QUANTUM ESPRESSO: a modular and open-source software project for quantum simulations of materials, *Journal of Physics: Condensed Matter* 21 (2009) 395502.
- [24] P. Giannozzi, O. Andreussi, T. Brumme, O. Bunau, M. B. Nardelli, M. Calandra, R. Car, C. Cavazzoni, D. Ceresoli, M. Cococcioni, N. Colonna, I. Carnimeo, A. D. Corso, S. de Gironcoli, P. Delugas, R. A. DiStasio, A. Ferretti, A. Floris, G. Fratesi, G. Fugallo, R. Gebauer, U. Gerstmann, F. Giustino, T. Gorni, J. Jia, M. Kawamura, H.-Y. Ko, A. Kokalj, E. Küçükbenli, M. Lazzeri, M. Marsili, N. Marzari, F. Mauri, N. L. Nguyen, H.-V. Nguyen, A. O. de-la Roza, L. Paulatto, S. Poncé, D. Rocca, R. Sabatini, B. Santra, M. Schlipf, A. P. Seitsonen, A. Smogunov, I. Timrov, T. Thonhauser, P. Umari, N. Vast, X. Wu, S. Baroni, Advanced capabilities for materials modelling with quantum ESPRESSO, *Journal of Physics: Condensed Matter* 29 (2017) 465901.
- [25] G. I. Csonka, J. P. Perdew, A. Ruzsinszky, P. H. T. Philipsen, S. Lebègue, J. Paier, O. A. Vydrov, J. G. Ángyán, Assessing the performance of recent density functionals for bulk solids, *Phys. Rev. B* 79 (2009) 155107.
- [26] M. De La Pierre, R. Orlando, L. Maschio, K. Doll, P. Ugliengo, R. Dovesi, Performance of six functionals (LDA, PBE, PBESOL, B3LYP, PBE0, and WC1LYP) in the simulation of vibrational and dielectric properties of crystalline compounds. the case of forsterite Mg_2SiO_4 , *Journal of Computational Chemistry* 32 (2011) 1775–1784.
- [27] A. V. Terentjev, L. A. Constantin, J. M. Pitarke, Dispersion-corrected PBESol exchange-correlation functional, *Phys. Rev. B* 98 (2018) 214108.
- [28] P. E. Blöchl, O. Jepsen, O. K. Andersen, Improved tetrahedron method for brillouin-zone integrations, *Phys. Rev. B* 49 (1994) 16223–16233.
- [29] S. Skaftouros, K. Özdoğan, E. Şaşıoğlu, I. Galanakis, Generalized slater-pauling rule for the inverse heusler compounds, *Phys. Rev. B* 87 (2013) 024420.
- [30] I. Galanakis, P. H. Dederichs, N. Papanikolaou, Slater-pauling behavior and origin of the half-metallicity of the full-heusler alloys, *Phys. Rev. B* 66 (2002) 174429.